IEEE Access
Multidisciplinary ⋮ Rapid Review ⋮ Open Access Journal

Received August 4, 2021, accepted August 8, 2021, date of publication August 12, 2021, date of current version August 19, 2021.

Digital Object Identifier 10.1109/ACCESS.2021.3104281

Gearbox Fault Diagnosis Using Multiscale Sparse Frequency-Frequency Distributions

LUKE ZHANG[1], YI LI[1], LINCHENG DONG[1], XIAOQING YANG[2,3], XIAOXI DING[2,3], (Member, IEEE), QIANG ZENG[3], LIMING WANG[2,3], AND YIMIN SHAO[3]

[1]Science and Technology on Reactor System Design Technology Laboratory, Nuclear Power Institute of China, Chengdu 610213, China
[2]College of Mechanical Engineering, Chongqing University, Chongqing 400044, China
[3]State Key Laboratory of Mechanical Transmission, Chongqing University, Chongqing 400044, China

Corresponding authors: Xiaoqing Yang (xqyang@cqu.edu.cn) and Xiaoxi Ding (dxxu@cqu.edu.cn)

This work was supported in part by the Central University Basic Research Fund under Grant 2020CDJGFCD002, and in part by the Chongqing Special Subsidies for Postdoctoral Research Projects under Grant XmT2020125.

ABSTRACT Gear fault related information is distributed over a broad frequency band, indicating a complex modulation mechanism. It is difficult to detect early-stage gear faults accurately by detecting fault frequencies in a limited frequency band. This paper proposes a novel method for achieving fault frequency detection more effectively. A short-frequency Fourier transform with a series of frequency-window functions is initially used to obtain the overall frequency information of a vibration signal. Subsequently, based on sparse decomposition and orthogonal matching pursuit, harmonic atoms are applied to refine modulation components from multiscale pseudo mono-components. A multiscale-sparse frequency-frequency distribution is eventually applied to augment existing fault-related harmonic components. In addition, a synthesized sparse spectrum is acquired by determining the frequency-frequency ridge from the multiscale sparse frequency-frequency distribution. Compared with empirical-mode-decomposition and fast-kurtogram analyses, the effectiveness and superiority of the proposed method for gear fault detection have been verified via experiments.

INDEX TERMS Demodulation, fault detection, Fourier transforms, gears, modulation, pursuit algorithms, sparse matrices, spectral analysis, vibrations, windows.

I. INTRODUCTION

Based on their key roles in rotating machines, gearboxes have been widely applied in industrial equipment such as automobiles [1], wind turbines [2], [3], etc. Unfortunately, as a result of unfavorable conditions and fluctuating loads during service, gearboxes are inevitably exposed to faults, which may result in enormous economic losses and security issues [4]. Therefore, the effective and timely fault diagnosis is crucial for preventing disasters.

However, gear fault diagnosis is challenging. Variable and harsh environments trigger localized defects such as cracking, spalling, or both. The diversity of these faults cause several difficulties in gear fault diagnosis. Additionally, the fault responses triggered by unavoidable manufacturing and assembly errors always modulate defect information in multiple frequency bands, indicating that there are various forms of modulation side-bands around the gear mesh frequency and its higher harmonics in the spectrum. Multi-modulations with multi-coupling phenomena further weaken the distribution characteristics of fault-related components to different degrees. To address these challenges, several methods have been developed to monitor gearbox conditions accurately. These methods primarily focus on three areas: mechanism analysis based on dynamic modelling [5]–[7], mathematical modelling [8], [9], and data-based monitoring [10]–[12].

Regarding dynamic mechanisms, transient impulses always exist as a result of periodic time-varying meshing stiffness and force that trigger interference for diagnosis analysis. By synthetically considering the characteristics of strong noise, weak fault signals, multi-modulation, and multi-coupling, it can be observed that sensitive information extraction from raw contaminated signals is important

The associate editor coordinating the review of this manuscript and approving it for publication was Gerard-Andre Capolino.

for gear fault diagnosis. Multiscale analyses, including the short time Fourier transform (STFT) [13], wavelet transform (WT) [14], [15], empirical mode decomposition (EMD) [16], and variational mode decomposition (VMD) [17], have been validated as effective tools for separating related modulated components. However, these applications of multiscale analyses are limited by their own peculiarities to different degrees. For example, the STFT cannot consider both time and frequency resolutions once the 2D time-frequency window is determined. Parey employed the WT to resolve angular domain averaged signals and implemented diagnosis for gearbox faults [18], but the noise reduction effect of the WT significantly depends on its mother wavelet. It is difficult to select a suitable mother wavelet that agrees well with the physical structures of analytical signals. Amarnath successfully diagnosed faults in helical gears using EMD-based intrinsic mode functions [19]. Owing to the endpoint effect and modal aliasing, EMD is unsuitable for analyzing complex modulated signals, and it also has weak theoretical support. Miao employed VMD to diagnose planetary gearbox faults and realized efficient and accurate effects for defect separation [20], but the denoising performance of VMD relies heavily on decomposition parameters that are difficult to determine and require prior knowledge. It should be noted that these methods all share two common limitations. First, they obtain partial sensitive bands within the entire frequency band, which induces the loss of meaningful information and yields unclear multiscale distribution characteristics. Second, they do not consider in-band noise, which is necessary for accurate fault diagnosis.

To address the limitations of existing multiscale analysis methods, a method called sparse representation has attracted significant research interest and exhibited promising performance for noise removal and mechanical fault diagnosis [21]–[24]. This method operates based on the diverse modulation distribution characteristics of faulty gears. Sun designed a parametric impulsive dictionary to address the problems of mutual coherence between atoms and low matching of atoms to signals [25], which improved calculation efficiency and impact feature extraction accuracy. However, this method only focuses on local faults, and its application to gear fault feature extraction must be further verified. Deng proposed a novel parametric dictionary design algorithm, that optimally matched the underlying fault impact characteristics of analyzed signals, but its anti-noise performance must be further improved [26]. Medina applied sparse representation in a dictionary learning approach to perform the accurate identification and classification of a gear fault dataset [27]. He designed two sub-dictionaries to separate the steady and impact modulations of gear compound faults. In addition, the effectiveness of this method was verified through simulations and experiments [28], [29], where he adopted the modulation feature in the resonance region to identify impact gear faults. Ding constructed a novel time-frequency impulsive atom and adopted its sparse representation for bearing fault diagnosis [30], which ignored the physical fault characteristics. Accordingly, mathematical model analysis of gearbox vibration signal can provide a sparse representation of the desired fault information, where the meshing characteristics of modulation information distributed in different frequency bands can be optimally extracted. However, existing model-driven methods based on sparse decomposition primarily focus on transient feature extraction while ignoring the steady modulation features distributed in full frequency bands, which hinders the accurate extraction of impact modulation components and accurate gear fault diagnosis.

This study aimed to realize a general fault frequency distribution to illustrate the complex modulation information systematically. Such information is disturbed by strong noise in a broad frequency range. First, a short-frequency window function is introduced to obtain multi-scale features through an FT (short-frequency FT, SFFT), where a series of pseudo mono-frequency components exists. Subsequently, a sparse representation with a mathematical model analysis of a gearbox is applied to each pseudo mono-frequency subsignal, where noise interference can be optimally eliminated from the envelope spectrum. Therefore, a new view of multiscale fault information can be provided in a sound spectrum called a multiscale sparse frequency-frequency distribution (MSFFD). Furthermore, a synthesized sparse spectrum (SSS) is applied to the MSFFD. Multiple types of modulation information can be mined efficiently and used to support accurate gear fault diagnosis. In contrast to the conventional multi-scale analysis method, the originality of the proposed method is to synthesize crucial sparse information distributed in a multi-scale modulation model for an effective identification effect. The vibration modulation model of gear faults is innovatively combined with sparse decomposition through the application of the SFFT and SSS, which adaptively utilize fault modulation information in the full frequency range to enhance the fault features of weak gear faults with high effectiveness. The proposed method is not limited to impact modulation signals within the resonance region and circumvents the sensitive band selection of gear faults involved in most conventional methods.

The remainder of this paper is organized as follows. Section 2 presents mathematical model analysis in the frequency and envelop spectrum. The theoretical background of the proposed MSFFD is also presented. In Section 3, experimental results and comparisons are used to verify the effectiveness of the proposed method for gear fault diagnosis. Finally, Section 4 summarizes our conclusions.

II. THEORETICAL BACKGROUND

In this section, we present transient signal analysis through parallel time-frequency filtering based on time-frequency modulation (TFM) signatures, which is called PTFM filtering. The proposed method faces two significant challenges. One is how to achieve theoretical reconstruction using an efficient TFM learning process because the conventional technique is very time consuming as a result of nonlinear learning. The second crucial challenge is how to apply the

local merits of TFM to global signals while retaining manifold morphology structures. The following sections primarily focus on these two challenges.

A. GEAR SIGNAL MODULATION MODEL

The meshing vibration of a typical gearbox can be approximated as a simple harmonic vibration and a measured signal $x(t)$ with N data points is primarily distributed in the change frequency of the meshing stiffness, which corresponds to the vibrations of meshing frequencies and their harmonics. Hence, it can be modelled as [8], [31]

$$x(t) = \sum_{m=0}^{M} A_m \cos(mw_z t + \phi_m) \tag{1}$$

$$w_z = 2\pi f_z, \quad w_r = 2\pi f_r, \quad f_z = zf_r \tag{2}$$

where A_m and ϕ_m represent the amplitude and phase of the mth mesh frequency component, respectively, and f_z and f_r are the meshing and rotating frequencies, respectively. In addition, M is the maximum order of the meshing frequency and r represents the shaft number. There are two main types of gear faults, namely distributed and local faults, which correspond to steady and impact modulations, respectively. Accordingly, the model can also be expressed as [22]

$$x(t) = x_d(t) + x_l(t) + \varsigma(t) \tag{3}$$

where $x_d(t)$, $x_l(t)$, and $\varsigma(t)$ represent the steady components, impact components, and noise, respectively. When a distributed/localized fault occurs, amplitude modulation and frequency/phase modulation emerge, along with variations in the meshing forces. In this study, we assumed that only amplitude modulation was available for gear vibration signals.

1) SIGNAL MODEL FOR FREQUENCY SPECTRUM ANALYSIS

For a distributed fault, the meshing frequency and harmonic components of the complex signal $x_d(t)$ can be rewritten as

$$\begin{aligned} x_d(t) &= \sum_{m=0}^{M} A_m \left[1 + b_m(t)\right] e^{i(mw_z t + \varphi_0)} \\ &= \sum_{m=0}^{M} A_m \left[1 + \sum_{k=0}^{K} B_{m,k} \cos(kw_r t)\right] e^{i(mw_z t + \varphi_0)} \end{aligned} \tag{4}$$

where K, φ_0, and $B_{m,k}$ represent the maximum order of the rotating frequency, initial phase, and modulation factor of the kth order rotating frequency of the mth mesh frequency component, respectively. It can be determined that the carrier frequencies include the meshing frequency and its harmonics $mw_z = mzw_r (m = 0, 1, 2, \ldots, M)$, whereas the modulation frequencies include the rotating frequency and its harmonics $kw_r (k = 0, 1, 2, \ldots, K)$.

Accordingly, based on the trigonometric function of amplitude modulation, the model in Eq. (4) can be transformed as

$$x_d(t) = \sum_{m=0}^{M} x_m(t) = \sum_{m=0}^{M} \sum_{k=0}^{K} \alpha_{m,k} e^{i[(mz \pm k)w_r t + \varphi_0]} \tag{5}$$

where $\alpha_{m,k}$ is the triangle coefficient. It can be observed that the raw distributed signal $x_d(t)$ can be decomposed into a series of mono-components with a mono-frequency sf_r, where order s is equal to $mz \pm k$ and is directly related to the rotating frequency f_r. The corresponding FT of $x_d(t)$ can be expressed as

$$X_d(w) = 2\pi \sum_{m=0}^{M} \sum_{k=0}^{K} \alpha_{m,k} \delta\left[w - (mz \pm k)w_r\right] \tag{6}$$

As a result of multiple modulation, the distributed fault information will appear in several mono-frequency scales $(mz \pm k)w_r$ with different modulating intensities $\alpha_{m,k}$. This suggests that we can extract and identify fault features at different frequency scales.

For a local fault, the impact frequency and harmonic components of the signal $x_l(t)$ can be rewritten as

$$g(t; w_l, \xi) = \begin{cases} e^{-\alpha[w_l t]^2} e^{iw_l t}, & |t| \le W \\ 0 & else \end{cases} \tag{7}$$

$$\begin{aligned} x_l(t) &= \sum_{p=-\infty}^{\infty} A_p g_p(t - p\tau_r) \\ &= g(t) * \sum_{p=-\infty}^{\infty} A_p \delta(t - p\tau_r) \end{aligned} \tag{8}$$

where A and $g(t; w_l, \xi)$ are the amplitude and impact form, respectively. Additionally, $w_l = 2\pi f_l$ represents the carrier frequency and τ_r denotes the period of transients, which is equal to $\tau_r = 1/f_r$. The impulse will periodically appear, and the FT of $x_l(t)$ is expressed as

$$\begin{aligned} X_l(w) &= G(w) \sum_{p=-\infty}^{\infty} A_p e^{-jpw\tau_r} \\ &\overset{A_p = constant}{=} \left\{ \frac{2\pi}{\sqrt{2\alpha w_l^2}} e^{-\frac{w^2}{4\alpha w_d^2}} * \delta(w - w_l) \right\} w_r \\ &\quad \times \sum_{p=0}^{\infty} a_p \delta(w \pm pw_r) \\ &= \frac{2\pi w_r}{\sqrt{2\alpha w_l^2}} e^{-\frac{w^2}{4\alpha w_l^2}} \sum_{p=0}^{\infty} a_p \delta\left[w - (w_l \pm pw_r)\right] \end{aligned} \tag{9}$$

According to this equation, it can be concluded that the transient fault feature $\sum_{p=0}^{\infty} a_p \delta(w \pm pw_r)$ will spread around the center frequency w_l in a limited frequency band $[w_l - Pw_r, w_l + Pw_r]$. The corresponding mono- frequency components $w_l \pm pw_r, (p = 0, 1, 2, \ldots, P)$ elucidate the transient characteristics, where P is the maximum order.

Therefore, according to Eqs. (3), (6) and (9), we can obtain the frequency spectrum of the gear signal $x(t)$ as

$$\begin{aligned} X(w) &= X_d(w) + X_l(w) + F_\varsigma(w) \\ &= F_\varsigma(w) + 2\pi \sum_{m=0}^{M} \sum_{k=0}^{K} \alpha_{m,k} \delta\left[w - (mz \pm k)w_r\right] \\ &\quad + \frac{2\pi w_r}{\sqrt{2\alpha w_l^2}} e^{-\frac{w^2}{4\alpha w_l^2}} \sum_{p=0}^{P} a_p \delta\left[w - (w_l \pm p w_r)\right] \end{aligned} \tag{10}$$

In addition, the fault features, including steady and impact modulations, will be carried by different frequencies mzw_r or w_l, and will concentrate on several mono-frequencies $(mz \pm k)w_r$ or $w_l \pm pw_r$ in limited frequency bands.

2) SIGNAL MODEL FOR FREQUENCY SPECTRUM ANALYSIS

The corresponding envelope spectrum for a given complex signal x(t) is also calculated as $E_x = ||x(t)||$. First, assuming that the components of signal x_d(t) correspond to the meshing frequency and its harmonics, a distributed fault signal, such as that modelled in Eq. (4), can be effectively separated through multi-scale analysis. Accordingly, the envelope spectrum of the separated component $x_d^m(t)$ can be obtained as

$$E_d^m = A_m \left[1 + \sum_{k=0}^{K} B_{m,k} \cos(k w_r t)\right], \quad m = 0, 1, \ldots, M \tag{11}$$

The fault information appears as a combination of harmonic signals related to the rotational frequency w_r. In addition, the corresponding frequency spectrum is obtained as

$$X_d^m(w) = A_m \left\{1 + \sum_{k=0}^{K} B_{m,k} \delta(w \pm k w_r)\right\}, \quad m = 0, 1, \ldots, M \tag{12}$$

For a local fault, as modelled in Eqs. (8) and (9), the corresponding envelope spectrum can be computed using Eq. (10) as follows

$$\begin{aligned} E_l &= E[x_l(t)] \\ &= E[g(t) * \sum_{p=-\infty}^{\infty} A_p \delta(t - p\tau_r)] \\ &= e^{-\alpha w_l^2 t^2} * \sum_{p=0}^{\infty} A_p \delta(t \pm p\tau_r) \end{aligned} \tag{13}$$

The corresponding frequency spectrum is obtained as

$$\begin{aligned} X_l(w) &= F\left[e^{-\alpha w_l^2 t^2}\right] F\left[\sum_{p=0}^{\infty} A_p \delta(t \pm p\tau_r)\right] \\ &\overset{A_p = constant}{=} \frac{w_r}{\sqrt{2\alpha w_l^2}} e^{-\frac{w^2}{4\alpha w_l^2}} \sum_{p=0}^{\infty} \delta(w \pm p w_r) \end{aligned} \tag{14}$$

The component $e^{-\alpha w_l^2 t^2}$ or $e^{-w^2/4\alpha w_l^2}$ is a Gaussian function and it serves as its own frequency spectrum. According to the monotonic decay property of the Gaussian function, it can be observed that the value of this component will continuously decrease until it disappears. Accordingly, a constraint condition can be set to ensure the maximum order of p as

$$e^{-\frac{w^2}{4\alpha w_l^2}} \geq \xi \Rightarrow w \leq 2\sqrt{\alpha \ln(1/\xi)} w_d \tag{15}$$

Because the value sequence for w is $pw_r (p = 0, 1, 2, \ldots, P)$, we can also obtain that

$$P \leq \frac{2\sqrt{\alpha \ln(1/\xi)} w_l}{w_r} \tag{16}$$

Therefore, by applying Eq. (15) to Eq. (14), we can obtain the limited form of the envelope spectrum as

$$\begin{aligned} X_l(w) &= \frac{w_r}{\sqrt{2\alpha w_d^2}} e^{-\frac{w^2}{4\alpha w_l^2}} \sum_{p=0}^{+\infty} \delta(w \pm p w_r) \\ &= \sum_{p=0}^{P} \left\{ \frac{w_r}{\sqrt{2\alpha w_l^2}} e^{-\frac{p^2 w_r^2}{4\alpha w_l^2}} \delta(w \pm p w_r) \right\} \end{aligned} \tag{17}$$

In conclusion, by using Eqs. (11) and (17), we can finally infer that the fault features hide in the envelope spectrum at each frequency scales, which can be uniformly expressed as a series of harmonic frequencies kw_r or pw_r with different distribution densities, including steady and impact faults.

$$d_{fscale}^{w_r, s} = \cos(s w_r t + \theta_s), \quad s = 0, 1, 2, \ldots, I \tag{18}$$

where w_r, I, and θ_s represent the rotational frequency of the gearbox, corresponding maximum order of the harmonic frequencies, and initial phase, respectively. In addition, f_{scale} represents the selected frequency scale for the component separated from the raw gear signal.

In general, the fault frequency w_r can be directly identified from the envelope spectrum E_x. However, owing to the multi-modulation and heavy interference noise, it is difficult to identify and extract fault features. Based on Eqs. (3), (4) and (9), we can conclude that the gear signal $x(t)$ can be considered a linear superposition of multiple components at different frequency scales, where different carrier waves combine different modulating waves. Hence, we can obtain the corresponding envelope as

$$\begin{aligned} E_x^2 &= \|x_d\|^2 + \|x_l\|^2 + (x_d \bar{x}_l + \bar{x}_d x_l) + E_\varsigma^2 \\ &= \sum_{m=0}^{M} \left\|x_d^m\right\|^2 + \|x_l\|^2 \\ &\quad + \sum_{\substack{i \neq j \\ i,j=0}}^{M} (x_d^i \bar{x}_d^j + \bar{x}_d^i x_d^j) + (x_d \bar{x}_l + \bar{x}_d x_l) + E_\varsigma^2 \end{aligned}$$

$$= \sum_{m=0}^{M} \left\|x_d^m\right\|^2 + \|x_l\|^2 + 2\sum_{\substack{i\neq j\\ i,j=0}}^{M} \left\|x_d^i x_d^j\right\| \cos(\theta_d^i - \theta_d^j)$$
$$+2\|x_d x_l\| \cos(\theta_d - \theta_l) + E_\varsigma^2$$
$$= \sum_{m=0}^{M} E_d^{m2} + E_l^2 + 2\sum_{\substack{i\neq j\\ i,j=0}}^{M} \left\|x_d^i x_d^j\right\| \cos(\nabla\theta_d^{i,j})$$
$$+2\|x_d x_l\| \cos(\nabla\theta_{d,l}) + E_\varsigma^2$$
$$= \sum_{m=0}^{M} E_d^{m2} + E_l^2 + E_{cross}^2 + E_\varsigma^2 \tag{19}$$

where $\nabla\theta_d^{i,j}$ represents the phase difference of the carrier frequencies izw_r and jzw_r, and $\nabla\theta_{d,l}$ denotes the phase difference of the carrier frequencies mzw_r and w_d. Therefore, we have

$$\begin{aligned}\nabla\theta_d^{i,j} &= m(i-j)w_r\\ \nabla\theta_{d,l} &= mzw_r - w_l\end{aligned} \tag{20}$$

By excluding the main components E_d^{m2} and E_l^2, it can be observed that several envelope cross-terms will emerge once multiple components (with different carrier frequencies mzw_r or w_d) appear in the raw signal. In this case, before calculating the envelope spectrum E_d^m or E_l, the raw signal $x(t)$ should be divided into a series of pseudo mono-components at different frequency scales, including the desired carrier frequency mzw_r or w_d. Accordingly, a series of pseudo mono-frequency components can be used to mine fault information, which will be discussed in the next section.

B. SHORT-FREQUENCY FOURIER TRANSFORM

According to the signal model for the frequency spectrum discussed in Sub-section 2.1.1, we can infer that the fault information of a defective gear will distribute over a wide frequency band, which is directly related to the carried frequencies, and that there are different modulating intensities for each frequency band. An important objective is to mine modulated information at different carrier frequency scales. In this section, a short- frequency window function is applied to the raw frequency spectrum to obtain multiscale frequency units. This method is called the SFFT, and aims to achieve multi-scale analysis for gear fault signals with multi-carrier frequencies.

A sliding window $g(\tau)$ centered at time t with a constant length of k is applied to the analysed time-domain signal $x(t)$, and the corresponding frequency information of the windowed time-domain signal $x_t(\tau) = x(\tau)g(\tau - t)$ can be analysed through an FT. Hence, the frequency distribution around the time shift t can be represented by the frequency spectrum of the modified signal $x_t(\tau)$ as

$$\begin{aligned}Y(t,w) = Y_t(w) &= \frac{1}{\sqrt{2\pi}}\int x_t(\tau)\mathrm{e}^{-jw\tau}\mathrm{d}\tau\\ &= \frac{1}{\sqrt{2\pi}}\int x(\tau)g(\tau-t)\mathrm{e}^{-jw\tau}\mathrm{d}\tau\end{aligned} \tag{21}$$

The STFT analyses the frequency characteristics at the time shift t. However, as mentioned in Subsection 2.1.1, the gear fault features of interest are distributed across different carrier frequency scales with different modulating intensities. Therefore, similar to the STFT with a time-domain filter used for analysing the frequency characteristics at the time shift t, the SFFT [22] focuses on applying a frequency-domain filter to study the time characteristics at the frequency scale w.

For a measured gear signal $x(t)$, the corresponding frequency spectrum is obtained from the FT as

$$X(w) = \frac{1}{\sqrt{2\pi}}\int x(t)\mathrm{e}^{-jwt}\mathrm{d}t \tag{22}$$

Similar to the time-domain window $g(\tau)$ in STFT, with a center frequency v and constant length W, a frequency-domain window $G(v)$ is employed to analyse the corresponding frequency-domain signal $X(w)$, which is defined as

$$X_w(v) = X(v)G(v-w) \tag{23}$$

It can be assumed that the frequency spectrum at the carrier frequency w only covers the modulated information carried by frequency w. Accordingly, the raw frequency features are fragmented into different carrier frequency scales. The corresponding time-domain signal of the windowed frequency-domain signal $X_w(v)$ at the frequency w can be calculated through a series of inverse FTs as

$$\begin{aligned}x(w,t) = x_w(t) &= \frac{1}{\sqrt{2\pi}}\int X_w(v)\mathrm{e}^{jvt}\mathrm{d}v\\ &= \frac{1}{\sqrt{2\pi}}\int X(v)G(v-w)\mathrm{e}^{jvt}\mathrm{d}v\end{aligned} \tag{24}$$

where $x(w,t)$ is a complex matrix, and a series of pseudo mono-frequency components $x_w(t)$ can be calculated at each frequency scale w. The definition of $E_w(t)$ for the corresponding amplitude density spectrum at the frequency shift w is expressed as

$$E_w(t) = E(w,t) = |x(w,t)| = |x_w(t)| \tag{25}$$

where a time-frequency distribution (TFD) can also be realized for time-frequency analysis. By using this SFFT-based TFD, we can obtain the multi-components for each carrier frequency scale, which elucidates the mono-frequencies $(mz \pm k)w_r$ or $w_d \pm pw_r$ modulated at different carrier frequencies mzw_r or w_d. For complex modulation, the desired fault characteristics will mainly be distributed in a limited frequency band, such as the frequency band $[-Iw_r, Iw_{r1}]$, where I is defined as the maximum order of the harmonics. In other words, the frequency extent with an available frequency bandwidth $2Iw_r$ can be covered by the frequency window function G. As illustrated in Fig. 1, the frequency spectrum can be divided into a series of modulation frequency bands, including the carrier frequencies mzw_r and w_d. A short frequency window with different frequency shifts is employed to obtain the local modulation band. In addition, the fault information can be further modulated from these narrow

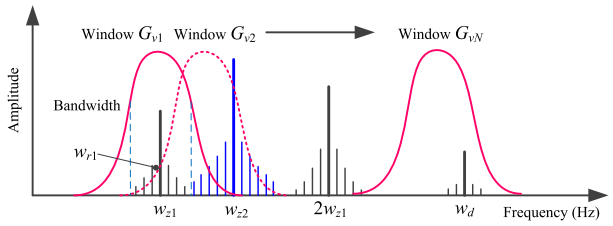

FIGURE 1. SFFT process with short-frequency window sliding in the frequency spectrum to divide the frequency spectrum into several modulation frequency bands. Here, mzw_r and w_d are the carried frequencies, and G represents the frequency window function.

bands at different frequency scales, where the cross terms in Eq. (19) can be ignored to a certain degree.

C. ORTHOGONAL MATCHING PURSUIT

By applying the introduced SFFT, a series of narrow-band signals, which contain multiple pseudo mono-frequency components can be derived. In addition, the SFFT-based TFD provides a method of amplitude density analysis for multi-frequency scales. Furthermore, considering the signal model for the envelope spectrum discussed in Subsection 2.1.2, we can also derive that the envelopes of the multiple pseudo mono-frequency components comprise harmonic waves related to rotational frequencies. As expressed in Eqs. (23)-(25), another crucial objective is to represent the envelope spectrum $F_w(t)$ sparsely, which facilitates the efficient mining of fault features. According to the principle of additional orthogonalization in the atom matching process, the orthogonal matching pursuit (OMP) technique is employed to match the crucial harmonic components to a given harmonic dictionary. For example, with a dictionary $\mathbf{d} = \{d_m, m = 1, 2, \ldots, n, ||d_i|| = 1\}$, a real signal $S \epsilon \, \mathrm{R}^L$ can be sparsely expressed by a linear combination of K atoms as

$$S = \sum_{k=1}^{K} g_{m_k} d_{m_k} \tag{26}$$

where m_k and g_{m_k} represent the label and coefficient of the matched atom d_{m_k}, respectively. To illustrate harmonic modulation, the dictionary $\mathbf{d}$ is defined as $\left\{ d_{f_{scale}}^{f_r,s} \middle| \cos(2\pi s f_r t + \theta_j), s = 0, 1, 2, \ldots, I, j = 0, 1, \ldots, J \right\}$ in Eq. (18), where f_r, I, and J represent the related rotational frequencies of all shifts, maximum order of the harmonic frequencies, and number of the initial phase in the range of $[0, 2\pi]$, respectively. Considering the non-stationarity and resolution ratio of the real signal, a frequency compensation factor Δf is introduced to extend $\pm 2\Delta f$. Therefore, as mentioned in Section 2.1, the raw envelope $F_w(t)$ can be decomposed into a series of harmonic atoms, where the approximation envelope $\hat{E}_w(t)$ is reconstructed and the residual error r_M is rejected. For the k-order approximation, the reconstructed envelope $\hat{E}_w(t)$ can be expressed as

$$\hat{E}_w^k(t) = \mathbf{d}_{fscale} c_k. \tag{27}$$

$$\mathbf{d}_{fscale} = \mathrm{supp}\{d_{fscale}^1, d_{fscale}^2, \ldots, d_{fscale}^k\} \tag{28}$$

$$c_k = \left(\mathbf{d}_{fscale}^T \mathbf{d}_{fscale} \right)^{-1} \mathbf{d}_{fscale}^T F_w(t) \tag{29}$$

where $\mathbf{d}_{fscale}$ and c_k are the matched dictionary and corresponding coefficient, respectively. In addition, the iteration termination condition can be ascertained from the energy ratio of the residual signal $r_i = E(t) - \hat{E}_w^i(t)$, which is expressed as

$$R_E = \frac{||r_{i+1}||^2 - ||r_i||^2}{||r_0||^2} < \xi \tag{30}$$

where ξ is a predetermined threshold.

D. MULTISCALE SPARSE FREQUENCY-FREQUENCY DISTRIBUTION

Based on the sparse representation of the envelope for each pseudo mono-frequency component, the Fourier spectrum at each frequency scale f_{scale} is derived for frequency-frequency analysis. We propose a novel frequency to frequency distribution called the multiscale sparse frequency-frequency distribution, which can be synthesized as

$$S(f_{scale}, f) = S_{fscale}(f) = \mathbf{F}\left[\hat{E}_{fscale}^k \right]\Big|_f \tag{31}$$

where $\hat{E}_{fscale}^k$ is the reconstructed envelope at the frequency scale f_{scale}. A multi-scale feature representation can be addressed using hard threshold de-noising, which is expressed as

$$S(f_{scale}, f) = \begin{cases} 0 & S(f_{scale}, f) \le \lambda \max\left[S(f_{scale}, f)\right] \\ S(f_{scale}, f) & else \end{cases} \tag{32}$$

Subsequently, it can be observed that a 2D distribution with multiscale frequencies retains all modulated information and fault characteristics, where substantial information can be explicitly expressed when different modulation levels are ignored.

For more comprehensive analysis, an SSS is derived through frequency-frequency ridge extraction from the MSFFD as

$$A(f) = \max_{f_{scale} \in All} S(f_{scale}, f) \tag{33}$$

As expressed in Eqs. (23) and (24), a series of pseudo mono-frequency components can be derived by applying the sliding operation of a frequency-domain window $G(v)$. As discussed for $G(v)$, which belongs to a weight sequence with time shifts, it can be inferred that the information at the frequency f_{scale} indicates a number of L_G (window length of the window function G) pseudo components. Therefore, an inverse weight at the scale f_{scale} is used to recalculate the sparse spectrum as

$$A_w(f) = \sum_{f_{scale}=Nf_1}^{Nf_2} \left[S_f(f_{scale}) / G(f_{scale} - f_{\max}^f) \right] \tag{34}$$

where Nf_1 and Nf_2 are the limited frequency points around the selected frequency scale ($\lfloor (Nf_2 + Nf_1)/2 \rfloor = f^f_{\max}$ and $Nf_2 - Nf_1 = L_G$). The weighted SSS synthetically provides a sound demodulation information distribution with multiple modulation. The proposed MSFFD aims to synthesize complex multiple modulation information and different modulation densities simultaneously. Additionally, it discards harmonic-unrelated noise to facilitate gearbox fault diagnosis.

E. PROCEDURE OF THE PROPOSED METHOD

Based on the sparse representation of vibration fault signals, the proposed MSFFD aims to represent pseudo mono-frequency components in multiple short frequency scales. Accordingly, a weighted sparse spectrum is obtained from the pseudo mono-components. A flowchart of the proposed method is illustrated in Fig. 2.

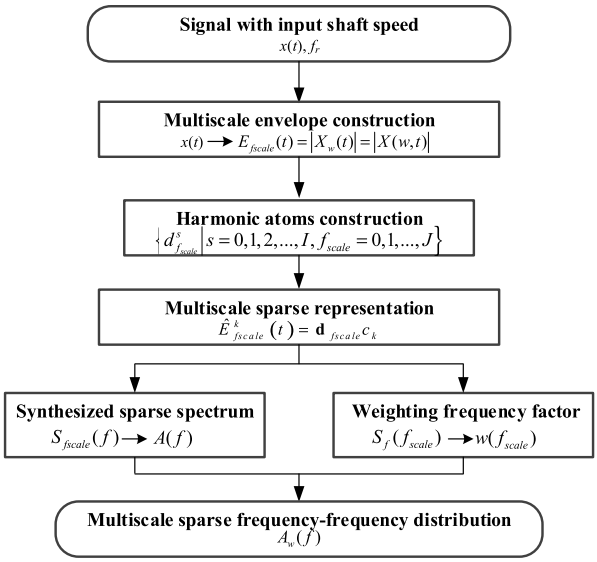

FIGURE 2. Illustration of the proposed MSFFD method containing multiple envelope construction, harmonic atoms construction, multiple sparse representation, synthesized sparse spectrum, weighting frequency factor, and multiple sparse frequency-frequency distribution.

For a gear fault vibration signal $x(t)$ with a rotation frequency of the input shaft of f_r, the MSFFD is implemented using the following four steps.

(I) The SFFT is first derived as expressed in Eq. (21), where the frequency-domain sliding window $G(v)$ is applied to obtain a series of pseudo mono-component signals from the frequency spectrum of $x(t)$, which involves different modulation densities. The corresponding envelops of the complex signal $x(w, t)$ cover the feature frequencies of interest.

(II) Based on the theoretical derivations for the gearbox vibration signal in Eqs. (4)-(20), harmonic atoms d^s_{fscale} are obtained using Eq. (18) under the condition of a known input shaft speed.

(III) Sparse coefficients are calculated based on the OMP technique using Eqs. (27)-(30) to obtain a sparse representation of the pseudo mono-components $\hat{E}^k_{fscale}(t)$. Subsequently, the frequency-to-frequency distribution $S(f_{scale}, f)$ can be acquired from the FT in Eqs. (31)-(32).

(IV) The synthesized sparse spectrum $A(f)$ is calculated from $S_{fscale}(f)$ using Eq. (33). The MSFFD is finally realized by fusing $A(f)$ and $w(f_{scale})$ using Eq. (34).

III. EXPERIMENTAL VALIDATIONS

A custom-made test stand for a gearbox driven system was used to verify the effectiveness of the proposed method. The test stand mainly consisted of a two-stage gearbox, magnetic powder brake, three-phase induction motor, control unit, and several flexible couplings, as presented in Fig. 3. The motor and magnetic powder brake are controlled by a frequency converter and load controller, respectively. The structural parameters of the two-stage gearbox are listed in Table 1, and the gear ratio of gearbox is approximately 3.59.

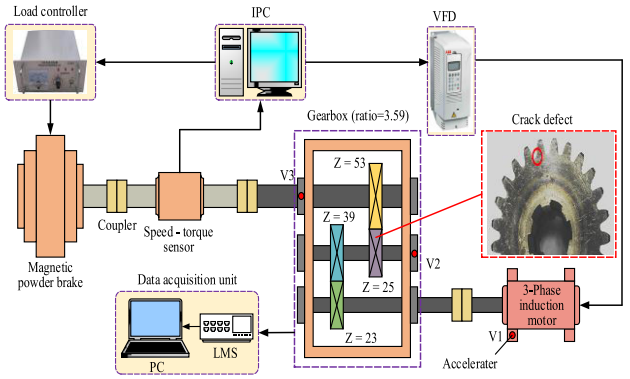

FIGURE 3. Custom-made test stand of two-stage gearbox testing system mainly comprising three-phase induction motor, gearbox, magnetic powder brake, data acquisition unit, load controller, coupler, speed-torque sensor, inter-process communication unit, and variable frequency drive.

TABLE 1. Structural parameters for the tooth numbers and gear ratios of the two-stage gearbox.

	First stage		Second stage	
	Driving gear	Driven gear	Driving gear	Driven gear
Tooth number	23		39	
Gear ratio	1.70		2.12	

Multiple operations with various speeds and loads can be tested using this gearbox system. With a 5120 -Hz sampling frequency, vibration signals are collected by a LMS data acquisition system with three accelerometers (V1/V2/V3) located in the bearing case of the gearbox, as illustrated in Fig. 3. A crack defect is conducted on the driving gear of the second-stage gear pair, as illustrated in Fig. 3. Owing to the relatively large bearing stiffness, and all the meshing excitations acting on the bearing pedestal, the vibration signals collected by the accelerometers on the bearings are typically larger than those elsewhere on the housing. The vibration signals collected by the accelerometer mounted on

the bearing pedestal of the intermediate shaft (location V2) were analysed, because the distances from the meshing points of the gearbox to V2 are more modest than V1 and V3, and accelerometer V2 can obtain vibration signals containing the fault information provided by each meshing point. The detailed frequency parameters of the gearbox can be calculated as presented in Table 2, where input speeds are 600, 800, 1000 and 1200 rpm, respectively. The fault characteristic frequency f_{sf} for the crack fault is equal to the shaft frequency of the middle shaft f_g, although they have different harmonic information.

TABLE 2. Frequency parameters (Hz) of the gearbox with different input speeds under the no-load condition.

Input speed / *rpm*	High-speed shaft in the first stage		Middle shaft	Low-speed shaft in the second stage	
	Shaft frequency f_h	Meshing frequency f_{m1}	Shaft frequency f_g	Shaft frequency f_h	Meshing frequency f_{m2}
600	10	230	5.90	2.78	147.44
800	13.33	306.67	7.86	3.71	196.58
1000	16.67	383.33	9.83	4.64	245.73
1200	20	460	11.79	5.56	294.87

A. EFFECTIVENESS OF THE PROPOSED METHOD

The time-domain waveforms of vibration signals are presented in Fig. 4 under different input speeds. These signals included impulse components. The vibration signal under the input speed of 600 rpm was analysed and the resulting spectrum is illustrated in Fig. 5(a). Evidently, the transient characteristic is completely submerged in the interference caused by strong noise and meshing components. According to the envelop spectrum in Fig. 5(b), frequency components such as f_g, f_h, and $2f_g$ are significant. However, some irrelevant elements still restrict the high harmonics of the shaft frequency. After applying the proposed method, the envelop spectrum is presented in Fig. 5(d). When comparing Figs. 5(b) and (d), it is clear that the proposed method is superior to the conventional demodulation method in terms of discarding interference elements. In Fig. 5(d), one can be observed that the f_g, f_h, and $2f_g$ components are more significant than the other components, which indicates that the gears mounted on the middle and input shafts, experienced faults. This agrees well with the crack on the driving gear of the second-stage gear pair. In addition, coupling often triggers the misalignment of the connection shaft, which causes misalignments of the input and output shafts. Hence, the harmonics of f_h in the envelop spectrum are triggered by the misalignment of the input shaft. In other words, the fault feature components are consistent with the experimental conditions.

Similarly, the vibration signals under input speeds of 800 rpm, 1000 rpm and 1200 rpm were also analysed using the spectrum analysis methods. Figs. 6(b) and (d) indicate that the fault feature harmonics in the envelope spectrum obtained by the proposed method are more dominant than those obtained by the compared method. Similar results can be observed in Figs. 7(b) and (d), which suggests that the

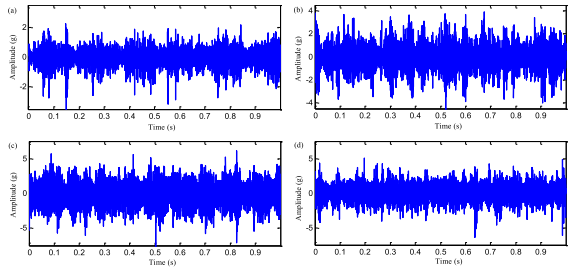

FIGURE 4. Waveforms of the gear crack defect signals under different input speeds: (a) 600 rpm, (b) 800 rpm, (c) 1000 rpm, and (d) 1200 rpm.

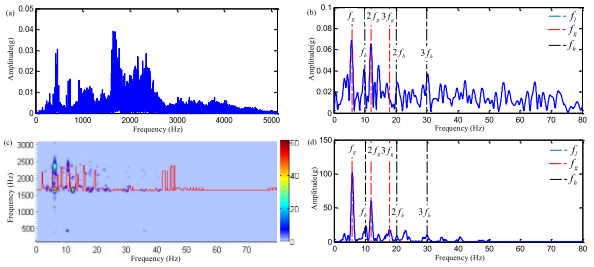

FIGURE 5. Spectrum analysis of the gear crack defect signal under an input speed of 600 rpm: (a) FFT spectrum, (b) envelop spectrum, (c) MSFFD (frequency ridge marked by red line), and (d) SSS (f_l, f_g, and f_h respectively correspond to the shaft frequencies of the output, middle and input shafts).

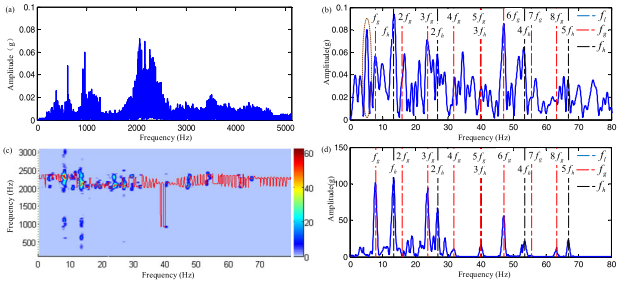

FIGURE 6. Spectrum analysis of the gear crack defect signal under an input speed of 800 rpm: (a) FFT spectrum, (b) envelop spectrum, (c) MSFFD (frequency ridge marked by red line), and (d) SSS (f_l, f_g, and f_h represent the shaft frequencies of the output, middle, and input shafts, respectively).

proposed method is more effective at enhancing fault feature components and discarding interference elements. It should be noted that f_l harmonics also emerge in the envelop spectrum, which coincides with the misalignment of the output shaft. Similar results can be observed in Fig. 8(d), which presents the fault feature frequencies of the input, middle and output shafts related to the cracked gear and misalignments. In addition, the proposed method can effectively discard the illusory modulation components marked by the green circles in Figs. 8 (b) and (d). Therefore, it can be inferred that the proposed method can effectively extract fault modulation components and detect gear faults.

B. COMPARISONS

To demonstrate the effectiveness of the proposed method further, EMD-based spectrum and fast-kurtogram analyses were

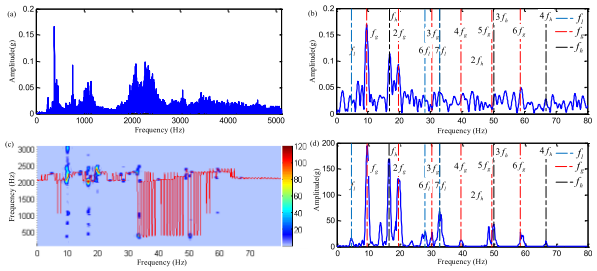

FIGURE 7. Spectrum analysis of the gear crack defect signal under a 1000-rpm input speed: (a) FFT spectrum, (b) envelop spectrum, (c) MSFFD (frequency ridge marked by red line), and (d) SSS (f_l, f_g, and f_h represent the shaft frequencies of the output, middle, and input shafts, respectively).

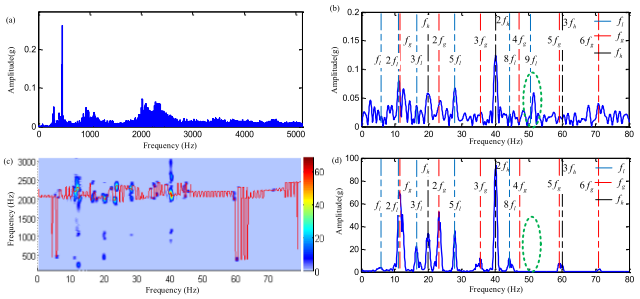

FIGURE 8. Spectrum analysis of the gear crack defect signal under a 1200 rpm input speed: (a) FFT spectrum, (b) envelop spectrum, (c) MSFFD (frequency ridge marked by red line), and (d) SSS (f_l, f_g, and f_h represent the shaft frequencies of the output, middle, and input shafts, respectively).

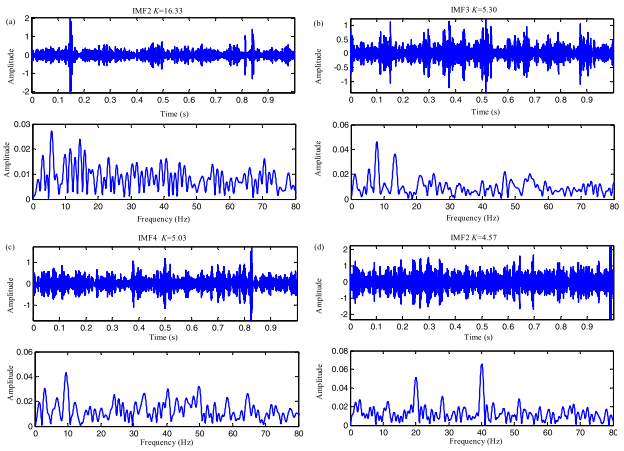

FIGURE 9. EMD-based spectrum analysis of the gear crack defect signals under different input speeds: (a) 600 rpm, (b) 800 rpm, (c) 1000 rpm, and (d) 1200 rpm.

adopted to assess the measured vibration signals. By comparing Figs. 9 and 10 to Figs. 5–8, it can be inferred that some fault feature components related to the gear faults cannot be clearly identified, which goes against the correct fault diagnosis. This comparison further validates the proposed method in terms of the accuracy of fault feature extraction from complicated modulation signal triggered by multiple gear faults.

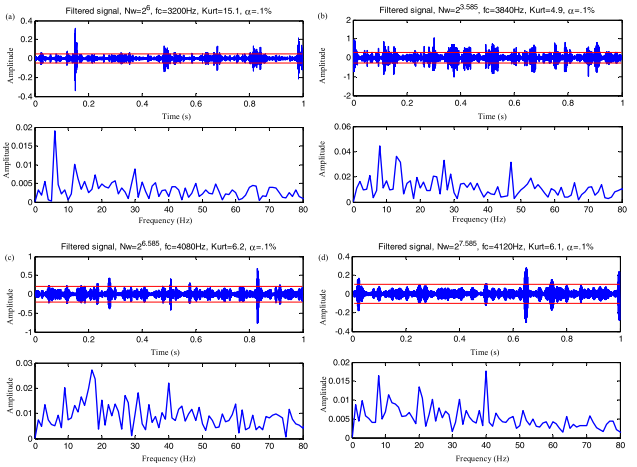

FIGURE 10. Fast-kurtogram analysis of the gear crack defect signals under different input speeds: (a) 600 rpm, (b) 800 rpm, (c) 1000 rpm, and (d) 1200 rpm.

IV. CONCLUSION

In the paper, a novel gear fault frequency detection method called MSFFD was proposed for gearbox fault diagnosis. First, a series of pseudo mono-components acquired by a frequency-window function are used to obtain the desired modulation features that are sparsely distributed in multi-scale space. Second, a weighted SSS synthetically provides efficient fault detection feature. Hence, the proposed method can extract multiple modulation components combined with different modulation levels at one frequency scale with a series of pseudo mono-components, which can clearly separate and sparsely represent fault-related harmonics to derive a logical and accurate fault frequency distribution. In addition, the weighted SSS can elucidate the weighted SSS structure of fault frequency components and detect gear faults. Experiments and comparisons verified the effectiveness of the proposed method at enhancing fault feature components, and demonstrated the advantages of the proposed method for obtaining information from multiple modulation signals for gear fault diagnosis. These results were confirmed through EMD-based spectrum and fast-kurtogram analyses. It should be noted that the quantifiable data on fault features are important for gear fault quantitative diagnosis, which should be further researched in the future to supplement gear fault quantitative diagnosis.

REFERENCES

[1] T. Praveenkumar, B. Sabhrish, M. Saimurugan, and K. I. Ramachandran, "Pattern recognition based on-line vibration monitoring system for fault diagnosis of automobile gearbox," *Measurement*, vol. 114, pp. 233–242, Jan. 2018.

[2] X. Chen and Z. Feng, "Time-frequency analysis of torsional vibration signals in resonance region for planetary gearbox fault diagnosis under variable speed conditions," *IEEE Access*, vol. 5, pp. 21918–21926, Oct. 2017.

[3] C. Cheng, X. Qiao, H. Luo, W. Teng, M. Gao, B. Zhang, and X. Yin, "A semi-quantitative information based fault diagnosis method for the running gears system of high-speed trains," *IEEE Access*, vol. 7, pp. 38168–38178, Mar. 2019.

[4] S. Tang, S. Yuan, and Y. Zhu, "Deep learning-based intelligent fault diagnosis methods toward rotating machinery," *IEEE Access*, vol. 8, pp. 9335–9346, Dec. 2020.
[5] G. He, K. Ding, X. Wu, and X. Yang, "Dynamics modeling and vibration modulation signal analysis of wind turbine planetary gearbox with a floating sun gear," *Renew. Energy*, vol. 139, pp. 718–729, Aug. 2019.
[6] K. Feng, W. A. Smith, P. Borghesani, R. B. Randall, and Z. Peng, "Use of cyclostationary properties of vibration signals to identify gear wear mechanisms and track wear evolution," *Mech. Syst. Signal Process.*, vol. 150, Mar. 2021, Art. no. 107258.
[7] Z. Shen, B. Qiao, L. Yang, W. Luo, Z. Yang, and X. Chen, "Fault mechanism and dynamic modeling of planetary gear with gear wear," *Mech. Mach. Theory*, vol. 155, Jan. 2021, Art. no. 104098.
[8] X. Yang, K. Ding, and G. He, "Phenomenon-model-based AM-FM vibration mechanism of faulty spur gear," *Mech. Syst. Signal Process.*, vol. 134, Dec. 2019, Art. no. 106366.
[9] X. Yu, Z. Feng, and M. Liang, "Analytical vibration signal model and signature analysis in resonance region for planetary gearbox fault diagnosis," *J. Sound Vib.*, vol. 498, Apr. 2021, Art. no. 115962.
[10] S. Xiang, Y. Qin, C. Zhu, Y. Wang, and H. Chen, "Long short-term memory neural network with weight amplification and its application into gear remaining useful life prediction," *Eng. Appl. Artif. Intell.*, vol. 91, May 2020, Art. no. 103587.
[11] C. Lv, P. Zhang, and D. Wu, "Gear fault feature extraction based on fuzzy function and improved Hu invariant moments," *IEEE Access*, vol. 8, pp. 47490–47499, Mar. 2020.
[12] Y. Qi, C. Shen, J. Zhu, X. Jiang, J. Shi, and Z. Zhu, "A new deep fusion network for automatic mechanical fault feature learning," *IEEE Access*, vol. 7, pp. 152552–152563, Oct. 2019.
[13] G. Manhertz and A. Bereczky, "STFT spectrogram based hybrid evaluation method for rotating machine transient vibration analysis," *Mech. Syst. Signal Process.*, vol. 154, Jun. 2021, Art. no. 107583.
[14] M. Gao, G. Yu, and T. Wang, "Impulsive gear fault diagnosis using adaptive Morlet wavelet filter based on alpha-stable distribution and kurtogram," *IEEE Access*, vol. 7, pp. 72283–72296, May 2019.
[15] X. Huang, G. Wen, L. Liang, Z. Zhang, and Y. Tan, "Frequency phase space empirical wavelet transform for rolling bearings fault diagnosis," *IEEE Access*, vol. 7, pp. 86306–86318, Jun. 2019.
[16] Y. Qin, "A new family of model-based impulsive wavelets and their sparse representation for rolling bearing fault diagnosis," *IEEE Trans. Ind. Electron.*, vol. 65, no. 3, pp. 2716–2726, Mar. 2018.
[17] J. Ding, D. Xiao, and X. Li, "Gear fault diagnosis based on genetic mutation particle swarm optimization VMD and probabilistic neural network algorithm," *IEEE Access*, vol. 8, pp. 18456–18474, Jan. 2020.
[18] A. Parey and A. Singh, "Gearbox fault diagnosis using acoustic signals, continuous wavelet transform and adaptive neuro-fuzzy inference system," *Appl. Acoust.*, vol. 147, pp. 133–140, Apr. 2019.
[19] M. Amarnath and I. P. Krishna, "Empirical mode decomposition of acoustic signals for diagnosis of faults in gears and rolling element bearings," *IET Sci., Meas. Technol.*, vol. 6, no. 4, pp. 279–287, Jul. 2012.
[20] Y. Miao, M. Zhao, Y. Yi, and J. Lin, "Application of sparsity-oriented VMD for gearbox fault diagnosis based on built-in encoder information," *ISA Trans.*, vol. 99, pp. 496–504, Apr. 2020.
[21] L. Wang, G. Cai, J. Wang, X. Jiang, and Z. Zhu, "Dual-enhanced sparse decomposition for wind turbine gearbox fault diagnosis," *IEEE Trans. Instrum. Meas.*, vol. 68, no. 2, pp. 450–461, Feb. 2019.
[22] N. Li, W. Huang, W. Guo, G. Gao, and Z. Zhu, "Multiple enhanced sparse decomposition for gearbox compound fault diagnosis," *IEEE Trans. Instrum. Meas.*, vol. 69, no. 3, pp. 771–781, Mar. 2020.
[23] Q. Li and S. Y. Liang, "Weak crack detection for gearbox using sparse denoising and decomposition method," *IEEE Sensors J.*, vol. 19, no. 6, pp. 22243–22253, Mar. 2019.
[24] N. Chai, M. Yang, Q. Ni, and D. Xu, "Gear fault diagnosis based on dual parameter optimized resonance-based sparse signal decomposition of motor current," *IEEE Trans. Ind. Appl.*, vol. 54, no. 4, pp. 3782–3792, Jul. 2018.
[25] R.-B. Sun, Z.-B. Yang, Z. Zhai, and X.-F. Chen, "Sparse representation based on parametric impulsive dictionary design for bearing fault diagnosis," *Mech. Syst. Signal Process.*, vol. 122, pp. 737–753, May 2019.
[26] F. Deng, Y. Qiang, S. Yang, R. Hao, and Y. Liu, "Sparse representation of parametric dictionary based on fault impact matching for wheelset bearing fault diagnosis," *ISA Trans.*, vol. 110, pp. 368–378, Apr. 2021.
[27] R. Medina, X. Alvarez, D. Jadán, J.-C. Macancela, R. Sánchez, and M. Cerrada, "Gearbox fault classification using dictionary sparse based representations of vibration signals," *J. Intell. Fuzzy Syst.*, vol. 34, no. 6, pp. 3605–3618, Jun. 2018.
[28] G. He, K. Ding, and H. Lin, "Gearbox coupling modulation separation method based on match pursuit and correlation filtering," *Mech. Syst. Signal Process.*, vols. 66–67, pp. 597–611, Jan. 2016.
[29] X. Yang, K. Ding, G. He, and Y. Li, "Double-dictionary signal decomposition method based on split augmented Lagrangian shrinkage algorithm and its application in gearbox hybrid faults diagnosis," *J. Sound Vib.*, vol. 432, pp. 484–501, Oct. 2018.
[30] Q. Li, X. Ding, Q. He, W. Huang, and Y. Shao, "Manifold sensing-based convolution sparse self-learning for defective bearing morphological feature extraction," *IEEE Trans. Ind. Informat.*, vol. 17, no. 5, pp. 3069–3078, May 2021.
[31] X. Yang, K. Ding, and G. He, "Accurate separation of amplitude-modulation and phase-modulation signal and its application to gear fault diagnosis," *J. Sound Vib.*, vol. 452, pp. 34–50, Jul. 2019.

LUKE ZHANG received the M.D. degree in mechanical engineering from Chongqing University, Chongqing, China, in 2020. He is currently working with Nuclear Power Institute of China. His research interests include signal processing and vibration reduction.

YI LI received the M.D. degree in mechanical engineering from Harbin Institute of Technology, Harbin, China, in 2015. He is currently working with Nuclear Power Institute of China. His research interest includes nuclear power device design.

LINCHENG DONG received the B.S. and Ph.D. degrees in mechanical engineering from Tianjin University, China, in 2014 and 2020, respectively. He is currently working with Nuclear Power Institute of China. His research interests include signal processing and vibration reduction.

XIAOQING YANG received the B.S. degree in mechanical engineering from Southwest Jiaotong University, in 2015, and the Ph.D. degree from South China University of Technology, China, in 2020. She is currently a Research Associate with the State Key Laboratory of Mechanical Transmission, Chongqing University, China. Her research interests include signal processing, equipment fault diagnosis, and gear system dynamics.

XIAOXI DING (Member, IEEE) received the B.S. and Ph.D. degrees in mechanical engineering from the University of Science and Technology of China, Hefei, China, in 2012 and 2017, respectively. He is currently a Research Associate with the State Key Laboratory of Mechanical Transmission, Chongqing University, China. His current research interests include signal processing, data mining, and intelligent monitoring system for health monitoring and fault diagnosis in machines.

QIANG ZENG received the B.S. and Ph.D. degrees in mechanical engineering from Chongqing University, Chongqing, China. He was sponsored by China Scholarship Council's Joint Ph.D. Program as a joint Ph.D. Student at the University of Huddersfield. He is currently a Research Associate in mechanical engineering with the State Key Lab of Mechanical Transmissions, Chongqing University. His research interests include signal processing, equipment fault diagnosis, data analysis, and pattern recognition.

LIMING WANG received the B.S. and Ph.D. degrees in machinery design, manufacturing and automation and mechanical engineering from Chongqing University, Chongqing, China, in 2011 and 2018, respectively. He is currently a Postdoctoral with the College of Mechanical Engineering, Chongqing University. He is also a Research Assistant with the State Key Laboratory of Mechanical Transmission, Chongqing University. His research interests include health condition monitoring for rotating machinery and fault diagnosis applications.

YIMIN SHAO received the B.S. degree in metallurgical machinery from the University of Science and Technology Beijing, China, in 1992, and the Ph.D. degree in production engineering specialist from the Gunma University, Japan, in 1997. From 1997 to 2004, he was a Research Associate with the Gunma University and a Visiting Scholar with the EU FP7 Marie Curie International Incoming Fellow, U.K., in 2012. He is currently a Professor and the Vice Director with the State Key Laboratory of Mechanical Transmissions, Chongqing University, Chongqing, China. His research interests include signal processing, noise analysis and pattern recognition, equipment fault diagnosis, intelligent monitoring and residual life prediction technology, precision transmission, and system integration technology.